Published in final edited form as:
Structure. 2008 June ; 16(6): 976–985. doi:10.1016/j.str.2008.02.025.

Structure of a Copper Pump suggests a Regulatory Role for its Metal Binding Domain

Chen-Chou Wu[1], **William J. Rice**[2], and **David L. Stokes**[1,2]

[1]Skirball Institute of Biomolecular Medicine, NYU School of Medicine, 540 First Ave., New York, NY 10016

[2]New York Structural Biology Center, 89 Convent Ave, New York, NY 10027

SUMMARY

P-type ATPases play an important role in Cu homeostasis, which provides sufficient Cu for metalloenzyme biosynthesis, but prevents oxidative damage of free Cu to the cell. The P_{IB} group of P-type ATPases includes ATP-dependent pumps of Cu and other transition metal ions; this group is distinguished from other family members by the presence of N-terminal metal binding domains (MBD). We have determined structures of two constructs of a Cu pump from *Archeaoglobus fulgidus* (CopA) by cryoelectron microscopy of tubular crystals, which reveal the overall architecture and domain organization of the molecule. By comparing these structures, we have localized its N-terminal MBD within the cytoplasmic domains that use ATP hydrolysis to drive the transport cycle. We have built a pseudo-atomic model by fitting existing crystallographic structures into the cryoelectron microscopy maps for CopA, which suggest a Cu-dependent regulatory role for the MBD.

INTRODUCTION

Copper is an essential cofactor for many enzymes but can also be toxic due to its potential to drive oxidation/reduction reactions and to form free radicals. Therefore, all living cells from bacteria to mammals have developed mechanisms to finely control intracellular Cu concentration (Vulpe and Packman, 1995). P-type ATPases compose one of the principal protein families involved in Cu homeostasis, which comprise a variety of ATP-dependent, transmembrane ion pumps and has been divided into a number of subgroups, denoted P_I-P_V (Axelsen and Palmgren, 1998). Cu transport is handled by the P_{IB} group, which also includes transporters of other transition metal ions, such as Zn^{2+}, Cd^{2+}, Co^{2+} and Pb^{2+} (Lutsenko and Kaplan, 1995; Williams and Mills, 2005). The best characterized P-type ATPases come from the P_{II} group and include mammalian Ca^{2+}-ATPase and Na^+/K^+-ATPase, which have been the subject of numerous cell biological, biochemical and structural studies (Kuhlbrandt, 2004).

In humans, two P_{IB} ATPases are responsible for maintaining appropriate Cu concentrations and, when defective, give rise to Menkes (MNK) and Wilson's (WNDP) diseases (DiDonato and Sarkar, 1997). They are found in the membrane of the trans golgi network but can be targeted to different cellular membranes in response to a variety of cellular signals (Lutsenko et al., 2007). In yeast, Ccc2p pumps Cu into the golgi (Yuan et al., 1997) and homologues have

Correspondence should be addressed to DLS: email: E-mail: stokes@nyu.edu; phone: 212-263-1580; fax: 646-219-0300.

also been characterized from plants to bacteria, for example OsHMA9 in *O. sativa* (Lee et al., 2007), CUA-1 in *C.elegans* (Yoshimizu et al., 1998), and either CopA or CopB in a variety of bacteria (Mandal et al., 2002; Odermatt et al., 1993; Rensing et al., 2000). In most cases, soluble metallochaperones have also been identified, which play a role in chelating free Cu in the cytoplasm and delivering it to the transporters (Pufahl et al., 1997).

Members of the P-type ATPase family are characterized by the formation of a phosphorylated intermediate during the enzymatic cycle, by a common membrane topology and domain organization, and by conserved sequence motifs implicated in ATP hydrolysis and phosphorylation (Kuhlbrandt, 2004; Moller et al., 1996). Based primarily on studies of P_{II} ATPases, the reaction cycle involves alternation between E1 and E2 states, in which transmembrane ion sites are oriented towards the intracellular or the extracellular milieu, respectively. A catalytic aspartate within the cytoplasmic domains can be phosphorylated in either state, which has a long-range conformational effect on the transmembrane domain and thus modulates accessibility of the ion transport sites therein. X-ray structures of the sarcoplasmic reticulum Ca^{2+}-ATPase (SERCA1a) have defined three cytoplasmic domains and demonstrated the conformational changes that accompany principle steps of enzymatic cycle (Moller et al., 2005; Toyoshima and Inesi, 2004). In particular, the N-domain binds ATP, the P-domain contains the catalytic aspartate, and the A-domain helps couple phosphorylation/dephosphorylation with ion site gating. P_{IB} ATPases retain these characteristics and are additionally equipped with a specialized N-terminal domain that carries characteristic metal binding domains (MBD). Although there are several atomic structures of P_{IB} ATPases, they all represent isolated cytoplasmic domains, i.e., N-domain (Dmitriev et al., 2006; Haupt et al., 2004), composite N- and P-domain (Lubben et al., 2007; Sazinsky et al., 2006b), A-domain (Sazinsky et al., 2006a), and N-terminal MBDs (Banci et al., 2002a; Banci et al., 2002b; Banci et al., 2004; Gitschier et al., 1998). To date, there is no structural information for an intact P_{IB} ATPase to elucidate the interaction of the MBDs with the rest of the molecule.

As many as six MBDs are arranged in tandem on the N-terminal tail of P_{IB} ATPases, which have a conserved sequence motif (GMTCxxC) and structural fold also found in the soluble metallochaperones (Arguello et al., 2007). The role of these MBDs is uncertain though there is evidence for their contribution to protein targeting in mammalian cells (Forbes et al., 1999; Petris et al., 1996; Schaefer et al., 1999) and to regulation of transport activity (Huster and Lutsenko, 2003). Their structural homology to soluble Cu^{+} metallochaperones has lead to the idea that MBDs mediate transfer of Cu^{+} from chaperone to the transport site on the pump. Although transport has indeed been demonstrated between metallochaperones and MBDs (Achila et al., 2006), no definitive evidence exists for transfer to the membrane transport sites. In fact, many bacterial pumps appear to be minimally affected by removal of their respective MBDs (Fan and Rosen, 2002; Mana-Capelli et al., 2003; Mandal and Arguello, 2003; Rice et al., 2006).

CopA is a Cu^{+}-dependent P_{IB} ATPase present in a variety of bacteria, which typically has a single MBD in the N-terminal tail. CopA from *Archaeoglobus fulgidus* is unusual in having a second MBD on its C-terminal tail (Mandal et al., 2002); however, truncation or mutation of this C-terminal MBD does not have a significant affect on activity (Mandal and Arguello, 2003; Rice et al., 2006). In the current study, we have determined the structural location of the N-terminal MBD of CopA from *A. fulgidus* using cryoelectron microscopy to analyze tubular crystals of two different constructs. In particular, we have compared structures of a construct lacking the C-terminal MBD (ΔC-CopA) with another construct lacking both N- and C-terminal MBDs (ΔNΔC-CopA). Thus, we have identified the location of the N-terminal MBD relative to the N-, P- and A-domains that have been shown to drive catalysis. In particular, difference maps show that the N-terminal MBD of CopA straddles the N-domain and the A-domain. By using the X-ray structure of Ca^{2+}-ATPase as a template, we docked atomic

coordinates corresponding to CopA cytoplasmic domains into our map and created a pseudo-atomic model for the intact CopA molecule. This model reveals a conformational change in CopA that is consistent with the use of a phosphate analogue (MgF_4^{2-}) for crystallization of ΔNΔC-CopA. In addition, the model suggests how the N-terminal MBD may be auto-inhibitory in the Cu-free state, leading to a model for Cu-dependent regulation of CopA activity.

RESULTS

Crystallization of CopA

The two constructs of CopA used for crystallization are shown schematically in Figure 1 together with a polyacrylamide gel of the respective protein preparations. One construct produced a truncation of the C-terminal tail immediately after the last transmembrane helix (ΔC-CopA), whereas the other produced truncations of both N-terminal and C-terminal tails (ΔNΔC-CopA). Previous studies have documented that various constructs of CopA from *A. fulgidus*, including those studied here, require elevated temperatures for maximal levels of ATPase activity, an observation which is consistent with their derivation from the genome of an extreme thermophile (Mandal et al., 2002;Rice et al., 2006). Similarly, we found that elevated temperatures (~50°C) greatly favored the production of tubular crystals with helical symmetry. Although 2D arrays were also observed at room temperature, the proportion of tubular crystals was far lower. For ΔC-CopA, tubular crystals were grown in the presence of the Cu^+ chelator BCDS at pH 6.1, which is analogous to the conditions used to stabilize the E_2 enzymatic state of SERCA1 (Takahashi et al., 2007;Toyoshima and Nomura, 2002). Tubular crystals of ΔNΔC-CopA grew under similar conditions with the addition of MgF_4^{2-}, a phosphate analogue that has been shown to stabilize the E_2-P state of SERCA1 (Toyoshima et al., 2004). In both cases, tubes were >10 μm long and were rather narrow, with diameters of 30 nm and 35 nm for ΔC- and ΔNΔC-CopA, respectively (Figure 2).

Fourier transforms from tubular crystals preserved in the frozen-hydrated state are characterized by a set of layer lines reflecting an underlying helical symmetry (Figure 2). Initially, these layer lines were assigned an arbitrary set of Miller indices and, ultimately, their helical selection rule was established by assigning a consistent set of Bessel orders (DeRosier and Moore, 1970). Similar to tubular crystals of SERCA1 and the nicotinic acetylcholine receptor, each construct of CopA produced a range of helical symmetries (Toyoshima and Unwin, 1990;Xu et al., 2002). For 3D reconstruction, we selected a group of tubes conforming to a single selection rule: for ΔC-CopA tubes the (1,0) and (0,1) layer lines had Bessel orders of 5 and -8 respectively, whereas for ΔNΔC-CopA tubes, these primary layer lines had Bessel orders of 7 and -11. Although the axial positions of layer lines were somewhat variable, the corresponding changes in unit cell parameters were less than 2% (Table 1), indicating that Fourier-Bessel components of tubes within these respective symmetry groups could be averaged prior to 3D reconstruction. In the averaged data sets from both ΔC-CopA and ΔNΔC-CopA tubes, the phase residuals were consistent with two-fold symmetry, which we therefore used to derive statistical measures of resolution. In particular, we used both two-fold related phase residuals and the Fourier Shell Correlation after applying a 180° rotation to the unit cell. Table 1 indicates that averaged data from ΔC-CopA tubular crystals have slightly better resolution than ΔNΔC-CopA, which we would judge to be ~17 Å.

Structure of CopA

Structures of both ΔC-CopA and ΔNΔC-CopA are characterized by a closely associated dimer (Figure 3 and Supplementary Figure 1). The physiological significance of this dimeric arrangement is uncertain as other members of the P-type ATPase family are known to be fully functional in the monomeric state (Jorgensen and Andersen, 1988). The boundaries of the bilayer were determined from the mean radial density distribution, which reveals two strong

peaks arising from the electron-dense phosphates composing the lipid headgroups (Supplementary Figure 2). The ΔC-CopA dimer (Figure 3A-C) fits within a cylinder 76 Å in diameter and 108 Å long. The cytoplasmic domains extend ~78 Å above the bilayer surface, whereas the extracellular domains are not resolved from the inner leaflet of the bilayer. The shape of the cytoplasmic domains is generally reminiscent of both Na^+,K^+-ATPase (Rice et al., 2001) and Ca^{2+}-ATPase (Zhang et al., 1998) in the E_2 conformation. Indeed, the cytoplasmic head-piece of all three molecules is roughly pear-shaped, though in the side view of ΔC-CopA (Figure 3B) there is a low-density hole appearing at the center of the cytoplasmic domains. A similar, though smaller hole was previously seen in Ca^{2+}-ATPase that had been labeled by FITC prior to crystallization (Xu et al., 2002). Although the dimensions of the ΔNΔC-CopA dimer are similar, the cytoplasmic domains are more closely associated, thus filling this hole and reducing the length of the pear-shaped cytoplasmic headpiece (Figure 3D-F).

Model for CopA

Our goal was to use these structures to build a pseudo-atomic model for CopA and thus to define the location of the N-terminal MBD. As a first step, we calculated a difference map between the cytoplasmic domains of ΔC-CopA and ΔNΔC-CopA. When plotted at 2.5σ, this difference map revealed three positive densities, labeled D1, D2 and D3 (Figure 4A-C), and one negative density occupying the hole in the middle of the headpiece (Figure 4G-I). Next, we fit atomic models derived from X-ray crystal structures of isolated CopA cytoplasmic domains to the maps (Figure 4D-F). To guide this fit, X-ray structures for the isolated N-/P-domain pair (Sazinsky et al., 2006b) and for the isolated A-domain (Sazinsky et al., 2006a) were aligned with a structure of Ca^{2+}-ATPase in the analogous E_2 conformation (Takahashi et al., 2007). After this alignment, these three cytoplasmic domains were then fitted as a rigid body into the cytoplasmic region of our ΔC-CopA (Supplemental Figure 3). To optimize this fit, the N-domain was rotated slightly (<10°) away from the A-domain to produce the structure shown in Figure 4D-F. A similar procedure was used for fitting ΔNΔC-CopA, except that the structure of Ca^{2+}-ATPase in the E_2-P conformation (Toyoshima et al., 2004) was used as a template for rigidbody docking and, in this case, the N-domain was rotated ~10° toward the A-domain (Supplementary Figure 3). These small adjustments to the N-domain are consistent with the demonstrated flexiblility of the loops connecting it to the P-domain and with the wide variety of angles observed in structures of Ca^{2+}-ATPase (Kuhlbrandt, 2004; Toyoshima and Inesi, 2004). Although we attempted automated docking of these domains using the program Chimera (Pettersen et al., 2004), it produced a non-physiological rotation of the N-/P-domain pair relative to the A-domain.

In light of these atomic models, the difference densities labeled D2 and D3 in Figure 4 are consistent with a conformational change in the N-domain, caused by its movement relative to the A-domain. This movement also contributes to the hole observed in the middle of the ΔC-CopA cytoplasmic headpiece and the corresponding negative difference density in that location. However, this conformational change fails to account for the larger difference density D1, which we believe to reflect the presence of the N-terminal MBD in ΔC-CopA but not in ΔNΔC-CopA. Indeed, unoccupied density is present in this region of the ΔC-CopA map (Figure 4D-F) but not in the density map of ΔNΔC-CopA (Figure 5G-I). To explore the plausibility of this assignment, we docked the X-ray structure for the N-terminal MBD from *Bacillus subtilis* CopA (Banci et al., 2002a) next to the A-domain of ΔC-CopA. Orientation of the C-terminus of this MBD towards the transmembrane represented an important constraint for this docking, though the shape of the MBD itself largely dictated its final orientation (Figure 5).

The transmembrane region in our maps was consistent with the presence of eight transmembrane helices, as predicted for CopA. Sequence analysis of of P_{IB} ATPases suggests

that six of these helices correspond to the first six transmembrane helices of P_{II} ATPases and that two additional helices have been added to the N-terminal end of the molecule (Lutsenko and Kaplan, 1995). Thus, we built the transmembrane portion of our CopA model by placing the first six transmembrane helices of Ca^{2+}-ATPase in locations dictated by an alignment of P-domains. Overall, these six helices fit relatively well within the transmembrane density of CopA, but left empty density within the transmembrane envelope. We were then able to fit two additional helices within this envelope near the Ca^{2+}-ATPase M1 helix. Based on sequence alignments, these extra two helices were initially assigned as M1-M2, but a recent study of CopA proteolysis suggests that they might instead follow the first transmembrane helix of P_{II} pumps, making them M2-M3 (Figure 1) (Hatori et al., 2007). Accordingly, we have assigned these additional helices as M2 and M3 in Figure 6, which shows the fit at two different sections through the membrane for both CopA constructs.

DISCUSSION

We have presented structures of two CopA constructs at 17 Å resolution which we have used as templates for constructing pseudo-atomic models. The structures differ in two respects, namely the ligands used for crystallization and the presence of the N-terminal MBD. Comparison of these two structures suggests that the N-terminal MBD is located within the cytoplasmic head and further suggests that CopA undergoes a conformational change that may be related to the presence of a phosphate analogue at the catalytic site.

Based on the modeling of our two structures, the N-terminal MBD of CopA appears to lie in between the N- and A-domains (Figure 7), which are conserved cytoplasmic domains found in all P-type ATPases. Although MBDs are unique to the P_{IB} subfamily, a small N-terminal domain precedes the first transmembrane helix of other P-type ATPases and generally consists of a pair of α-helices. In the x-ray structures of Ca^{2+}-ATPase (Toyoshima et al., 2000), Na^+/K^+-ATPase (Morth et al., 2007) and H^+-ATPase (Pedersen et al., 2007), this pair of α-helices binds to the distal part of the β-barrel that constitutes the A-domain (e.g. Supplementary Figure 3E). An 10-15 residue unstructured loop connects these two α-helices to M1. This N-terminal domain forms an integral part of the A-domain and does not become displaced during the various conformational changes that accompany the catalytic cycle of Ca^{2+}-ATPase. Indeed, flexibility in the unstructured loop is essential for the dramatic movements of the A-domain during this cycle. On the other hand, the tugging of this loop on M1 is thought to initiate closing of the cytoplasmic ion gate upon formation of the high-energy phosphoenzyme (E1~P) (Sorensen et al., 2004;Toyoshima and Mizutani, 2004). A recent proteolysis study of CopA from *T. maritima*, suggested that its N-terminal MBD also formed an integral part of the A-domain and that the first transmembrane helix was analogous to the bent M1 helix seen in structures of Ca^{2+}-ATPase, Na^+/K^+-ATPase and H^+-ATPase (Hatori et al., 2007). This study also concluded that the two extra transmembrane helices at the N-terminus of CopA are inserted between M1 and M2 of Ca^{2+}-ATPase. Our structural analysis of CopA from *A. fulgidus* is consistent with these hypotheses, though the binding site of the N-terminal MBD on the A-domain is quite different from the two N-terminal helices of the other P-type ATPases. Our sequence alignments indicate that there are ~11 residues between the last β-strand of the N-terminal MBD from *A. fulgidus* CopA and the bent M1 helix (Supplementary Figure 4), which if extended could readily span the corresponding distance in our model. It should be noted, however, that the putative locations of M2 and M3 in our model could also be reached by this linker and that this plausible assignment for M1 must therefore remain tentative.

Although the resolution of our map is relatively low, the envelope constrains the location of the N-terminal MBD relative to the other cytoplasmic domains to a considerably higher degree. The legitimacy of this modeling approach has been demonstrated for both Ca^{2+}-ATPase (Xu et al., 2002) and Na^+/K^+-ATPase (Rice et al., 2001), for which pseudo-atomic models created

in a similar fashion were subsequently confirmed by X-ray crystallographic structures. The βαββαβ fold of MBDs consists of two α-helices packed against a four-stranded β-sheet and fits nicely within unoccupied density between the N- and A-domains (Figures 4 and 5). The Cu-binding GMTCxxC motif lies in the loop following the first α-helix, which caps a hydrophobic core between the sheet and the helices. According to our fit, the side of the N-terminal MBD packs against the side of the A-domain and the Cu-binding GMTCxxC loop interacts with the N-domain (Figure 7). Interestingly, the site of this N-domain interaction involves the ERRSEHP^{463} loop, which is highly homologous in MNK and WNDP pumps, where it has been implicated in ATP binding (Dmitriev et al., 2006; Morgan et al., 2004). The α-helical surface of the MBD is solvent exposed, which would potentially allow for its interaction with metallochaperones. Indeed, charged residues on this surface have been implicated in mediating the interaction and defining the specificity of MBD with its corresponding metallochaperone (Arnesano et al., 2004; Arnesano et al., 2002; Wernimont et al., 2000).

Previous work on P_{IB} ATPases have proposed two different roles for the MBDs. The human MNK and WNDP pumps have six tandem MBDs (MBD1-6). The first four appear to regulate activity by modifying the binding of ATP to the pump in a Cu-dependent manner (Huster and Lutsenko, 2003). Specifically, direct binding has been shown between the N-terminal MBDs and the ATP-binding domain of WNDP in a way that suggests autoinhibitory behavior of these MDBs in the absence of Cu and relief from this inhibition in the presence of Cu (Tsivkovskii et al., 2001). In contrast, mutations to MBD5 or 6 alter the apparent affinity of the intramembrane Cu transport sites (Huster and Lutsenko, 2003), though the mechanism for this effect is unclear. Cu transfer has been demonstrated from the metallochaperone Atox1 to MBD1-4 and also from MBD4 to MBD5,6 (Achila et al., 2006) and can be explained by a sequential exchange of cysteine ligands at the exposed Cu-binding sites (Wernimont et al., 2000). However, the transport sites are buried within a group of packed transmembrane helices and it is hard to envision how direct transfer from an MBD could be accomplished. Furthermore, all the bacterial P_{IB} ATPases appear functional in the absence of their N-terminal MBDs (Bal et al., 2001; Fan and Rosen, 2002; Mana-Capelli et al., 2003; Mandal and Arguello, 2003; Mitra and Sharma, 2001; Rice et al., 2006), suggesting that the more likely explanation is that Cu binding to these MBDs exerts an allosteric effect on global protein conformation, thus facilitating Cu binding to the transport sites.

Considering this work in the context of our CopA structure leads us to propose the following model. Like other P-type ATPases, the N-terminal MBD appears to be an integral part of the A-domain. In the Cu-free state, the MBD interacts with the N-domain and either prevents ATP binding or prevents the domain movement necessary to transfer the γ-phosphate to the catalytic aspartate, thus producing an autoinhibited state. Recognition of the MBD by Cu-loaded metallochaperone disrupts this interaction and leads to transfer of Cu to the MBD. Once loaded with Cu, the MBD is no longer able to interact with the N-domain, thus allowing ATP-binding, transfer of γ-phosphate and subsequent steps for Cu transport. This could explain the observation of substantially reduced activity of CopA caused by mutations in the CxxC motif that presumably prevent binding of Cu to the N-terminal MBD (Mandal and Arguello, 2003). It is not clear from our work so far whether the MBD remains associated with the A-domain in the Cu-bound state, or is able to swing down and dock at some location next to the membrane in order to deliver its Cu to the transport sites.

We used different conditions for crystallization of our two CopA constructs, which can be expected to induce different intermediates in the reaction cycle. In particular, ΔC-CopA was crystallized in the presence of Cu chelator (BCDS), whereas ΔNΔC-CopA required the addition of the phosphate analogue MgF_4^{2-} in addition to this chelator. These conditions were chosen empirically in order to optimize crystallization, but they also allow us to evaluate potential conformational changes of CopA that accompany the transition between the respective reaction

intermediates. In the case of Ca^{2+}-ATPase, X-ray crystal structures have been reported for the analogous intermediates, termed E2 for the chelator (EGTA) alone (Takahashi et al., 2007; Toyoshima and Nomura, 2002) and E2-P upon the addition of MgF_4^{2-} (Toyoshima et al., 2004). Although the membrane domains of the two structures are comparable, there are distinct differences in the cytoplasmic domains caused by the presence of the phosphate analogue. Specifically, the A- and P-domains are more tightly packed in the E2-P conformation due to the role of the conserved TGES loop within the A-domain in orienting a water molecule for hydrolysis of the aspartyl phosphate in the P-domain. In the absence of phosphate, there are no specific ligands holding the A-domain close to the catalytic site, allowing the two domains to move apart (Moller et al., 2005; Toyoshima and Inesi, 2004). Comparison of our CopA structures reveals a similar structural difference, with the cytoplasmic domains of ΔNΔC-CopA in the presence of MgF_4^{2-} being tightly packed whereas the structure ΔC-CopA actually has a low-density hole separating the A- and P-domains. The presence of the MBD in the latter structure is also likely to influence the domain interactions and, in the latter case, to pry to A-domain away from the N- and P-domains. MgF_4^{2-} substantially improved crystal order of ΔNΔC-CopA, suggesting that its ability to stabilize the A-/P-domain interface was an important factor. In contrast, MgF_4^{2-} interfered with crystallization of ΔC-CopA, implying a competition between MgF_4^{2-} binding and the MBD-stabilized state. Such a competition is consistent with our proposed role for the Cu-free MBD in preventing the necessary domain interaction and thus promoting an autoinhibited state.

EXPERIMENTAL PROCEDURES

CopA constructs

Two CopA constructs were used for crystallization (Figure 1). The first involved truncation of 68 residues from the C-terminus (ΔC-CopA) and the other involved a double truncation of the C-terminus together with 95 residues from the N-terminus (ΔNΔC-CopA). These truncations were designed to interrupt the native protein immediately adjacent to the respective transmembrane helix. Expression plasmids (pBAD) containing CopA constructs with histidine tags were obtained as described previously (Rice et al., 2006).

Protein expression and purification

E.coli (LMG1940) transformed with plasmids containing CopA constructs was cultured in LB broth with 0.1 mg/ml ampicillin at 37°C. After growing to an OD of 1, expression was induced with 0.02% arabinose for 2 h at 30°C before harvesting cells by centrifugation at 10,000g for 10min at 4°C. The pellet was suspended in a buffer composed of 50 mM Tris-Cl, pH 7.5, 20% glycerol, 50mM NaCl, 2mM β-mercaptoethanol, 0.05 mg/ml DNAse I and complete protease inhibitor cocktail (Roche) according to manufacturer's instructions. Cell membranes were broken by French Press at 20,000 psi and debris was removed by centrifugation at 12,000g for 20min at 4°C. Membranes were then collected by centrifugation at 150,000g for 1h at 4°C and stored at -80°C.

Membrane pellets were resuspended in a standard buffer (25 mM Tris-Cl, pH 7.5, 100mM NaCl, 10% glycerol, 2mM β-mercaptoethanol) with 20mM imidazole, EDTA-free protease inhibitor cocktail and 10 mg/ml dodecylmaltoside (DDM) at a total protein concentration of 10mg/ml. After gently mixing for 30 min at 4°C, insoluble material was removed by centrifugation at 150,000g for 30min at 4°C. The protein supernatant was then loaded onto a 5 ml HiTrap Chelating HP column (GE Healthcare), which was charged previously with 0.1 M $NiCl_2$ and equilibrated with standard buffer supplemented with 20mM imidazole and 0.1 % DDM. After washing, purified CopA protein was eluted with standard buffer supplemented with 400mM imidazole and 0.1 % DDM. The His-tag was removed from CopA by overnight incubation with 1 unit thrombin per mg of protein at 4°C. Thrombin was then removed with a

benzamidine-Sepharose column (Amersham Biosciences) equilibrated with standard buffer with 0.1 % DDM. Finally, CopA was dialyzed against 25mM Tris-Cl, pH7.5, 100mM Na_2SO_4, 10% glycerol, 2mM DTT and 0.1% DDM. Protein concentration was determined by absorbance at 280 nm. This procedure typically produced 5-8 mg of purified protein from 6 L of bacterial media. SDS-PAGE showed that the samples were >95% pure and thus suitable for crystallization trials (Figure 1).

Crystallization and electron microscopy

Tubular crystals of ΔC-CopA were grown by adding dioleoylphosphatidylcholine (0.4 mg per mg protein) and dialyzing the resulting protein mixture (0.5mg/ml total protein in 50μl dialysis button) against 50mM MES, pH 6.1, 25mM Na_2SO_4, 25mM K_2SO_4, 200μM BCDS, 10mM $MgSO_4$ and 2mM β-mercaptoethanol for 5 days at 45-55°C. Tubular crystals of ΔNΔC-CopA were grown under similar conditions except that 1mM NaF was added to the dialysis buffer. For electron microscopy, a suspension of crystals was deposited on a holey carbon grid and rapidly frozen in liquid ethane. Samples were imaged at -175°C with a CT3500 cryoholder (Gatan UK) at 50kx magnification with a CM200 FEG electron microscope (FEI Corp.) operating at 200 kV. Defocus values ranged from 9000 – 25000 Å. Electron micrographs were recorded on film and, after screening by optical diffraction, suitable images were digitized at 14-μm intervals with a Zeiss SCAI microdensitometer (Intergraph Corp.).

Image analysis

Helical reconstruction was carried out as previously described (Stokes et al., 2005; Xu et al., 2002). The helical symmetry was determined by assigning Bessel orders to principal layer lines labeled as (1,0) and (0,1) in Figure 2. The initial assignment was based on the expected location of the first maximum of the corresponding Bessel function $J_n(2\pi Rr)$, where n is the Bessel order, R is the observed distance of the first maximum along the layer line from the meridian, and r is the radius of the tube in real space. These initial assignments were checked in several ways. First, the phases of peaks across the low-lying layer lines should be equal for even Bessel orders or differ by 180° for odd Bessel orders. Second, the Bessel orders for other layer lines could be predicted from the principal layer lines and the distance of their initial peaks from the meridian should be consistent with these predictions. Finally, the determination of out-of-plane tilt is sensitive to these Bessel order assignments and the correct indexing scheme inevitably produced the lowest phase residual after applying the corresponding corrections (DeRosier and Moore, 1970). Handedness of the helical lattice was determined by tilting samples ~30° about an axis normal to the long axis of the tubes and analyzing the diffraction patterns from the left-half and right-half of the resulting images (Finch, 1972). Thus, the layer line designated as 1,0 (Figure 2) was determined to be right -handed. Several helical symmetry groups were found for both ΔC-CopA and ΔNΔC-CopA tubes (Toyoshima and Unwin, 1990) but only those with the selection rules shown in Figure 2 were used for further analysis. Each of these datasets were analyzed by the methods of Beroukhim and Unwin (Beroukhim and Unwin, 1997). Correction for the contrast transfer function was based on an amplitude contrast of 7% (Toyoshima et al., 1993). For the final maps, a Butterworth filter was applied using SPIDER (Frank et al., 1996) with pass-band and stop-band frequency of 13.3 Å and 9.5 Å respectively.

For calculation of a difference map, the cytoplasmic domains of the two maps were isolated and an isodensity contour was chosen to provide the expected volume for ΔC-CopA, assuming the value of 1.21 $Å^3$ per dalton (Harpaz et al., 1994). The density values for ΔNΔC-CopA were then scaled such that the same isodensity contour gave the expected volume, taking into account the missing N-terminal MBD. After scaling, the dimer was masked from each map, aligned and a simple subtraction was performed using SPIDER.

Docking of atomic coordinates

An initial model for CopA was created by superimposing atomic coordinates of N-/P-domain pair (2B8E) (Sazinsky et al., 2006b) and the A-domain (2HC8) (Sazinsky et al., 2006a) onto the X-ray crystallographic structure of Ca^{2+} ATPase in either the E2 (2EAR) (Takahashi et al., 2007) or E2-MgF_4^{2-} (1WPG) (Toyoshima et al., 2004) conformation (Supplemental Figure 3) using the MatchMaker routine in Chimera (Pettersen et al., 2004). The transmembrane domain was initially modeled as the first six helices from Ca^{2+}-ATPase. The resulting CopA models were then docked manually into the density maps. To optimize the fit, the N-domain and A-domain were adjusted slightly to match the map density and two additional helices, derived from Ca^{2+}-ATPase M7 and M10 were placed into the transmembrane domain. Finally, the N-terminal MBD from *B. subtilis* (1JWW) (Banci et al., 2002a) was placed into the map to occupy unassigned density in the cytoplasmic headpiece. The model was initially fitted to a monomer of CopA, whose boundaries were quite evident from the map (see Figure 3). The model was then duplicated and manually manipulated to fit into the two-fold related symmetry partner. No significant steric clashes resulted from placing this second molecule within the dimeric density, providing added confidence in the fit.

Supplementary Material

Refer to Web version on PubMed Central for supplementary material.

ACKNOWLEDGEMENTS

The authors would like to acknowledge Aleksandra Kovalishin for early work in expression and purification of CopA. The maps have been deposited in the EM Data Bank (EMDB) under the accession number EMD-5004 and the corresponding atomic models have been deposited in the Protein Data Bank (PDB) under accession numbers XXXXX. This research utilized the facilities at the New York Structural Biology Center, which is a STAR center supported by the New York State Office of Science, Technology, and Academic Research and was supported by NIH grant GM56950 to D.L.S.

REFERENCES

Achila D, Banci L, Bertini I, Bunce J, Ciofi-Baffoni S, Huffman DL. Structure of human Wilson protein domains 5 and 6 and their interplay with domain 4 and the copper chaperone HAH1 in copper uptake. Proc. Nat. Acad. Sci 2006;103:5729–5734. [PubMed: 16571664]

Arguello JM, Eren E, Gonzalez-Guerrero M. The structure and function of heavy metal transport P1B-ATPases. Biometals 2007;20:233–248. [PubMed: 17219055]

Arnesano F, Banci L, Bertini I, Bonvin AM. A docking approach to the study of copper trafficking proteins; interaction between metallochaperones and soluble domains of copper ATPases. Structure 2004;12:669–676. [PubMed: 15062089]

Arnesano F, Banci L, Bertini I, Ciofi-Baffoni S, Molteni E, Huffman DL, O'Halloran TV. Metallochaperones and metal-transporting ATPases: a comparative analysis of sequences and structures. Genome Res 2002;12:255–271. [PubMed: 11827945]

Axelsen KB, Palmgren MG. Evolution of substrate specificities in the P-type ATPase superfamily. J. Mol. Evol 1998;46:84–101. [PubMed: 9419228]

Bal N, Mintz E, Guillain F, Catty P. A possible regulatory role for the metal-binding domain of CadA, the Listeria monocytogenes Cd^{2+}-ATPase. FEBS Lett 2001;506:249–252. [PubMed: 11602255]

Banci L, Bertini I, Ciofi-Baffoni S, D'Onofrio M, Gonnelli L, Marhuenda-Egea FC, Ruiz-Duenas FJ. Solution structure of the N-terminal domain of a potential copper-translocating P-type ATPase from Bacillus subtilis in the apo and Cu(I) loaded states. J. Mol. Biol 2002a;317:415–429. [PubMed: 11922674]

Banci L, Bertini I, Ciofi-Baffoni S, Finney LA, Outten CE, O'Halloran TV. A new zinc-protein coordination site in intracellular metal trafficking: solution structure of the Apo and Zn(II) forms of ZntA(46-118). J. Mol. Biol 2002b;323:883–897. [PubMed: 12417201]

Banci L, Bertini I, Del Conte R, D'Onofrio M, Rosato A. Solution structure and backbone dynamics of the Cu(I) and apo forms of the second metal-binding domain of the Menkes protein ATP7A. Biochemistry 2004;43:3396–3403. [PubMed: 15035611]

Beroukhim R, Unwin N. Distortion correction of tubular crystals: Improvements in the acetylcholine receptor structure. Ultramicroscopy 1997;70:57–81. [PubMed: 9440347]

DeRosier DJ, Moore PB. Reconstruction of three-dimensional images from electron micrographs of structures with helical symmetry. J. Mol. Biol 1970;52:355–369. [PubMed: 5485914]

DiDonato M, Sarkar B. Copper transport and its alterations in Menkes and Wilson diseases. Biophys. Bioch. Acta 1997;1360:3–16.

Dmitriev O, Tsivkovskii R, Abildgaard F, Morgan CT, Markley JL, Lutsenko S. Solution structure of the N-domain of Wilson disease protein: distinct nucleotide-binding environment and effects of disease mutations. Proc. Nat. Acad. Sci 2006;103:5302–5307. [PubMed: 16567646]

Fan B, Rosen BP. Biochemical characterization of CopA, the Escherichia coli Cu(I)-translocating P-type ATPase. J. Biol. Chem 2002;277:46987–46992. [PubMed: 12351646]

Finch JT. The hand of the helix of tobacco virus. J. Mol. Biol 1972;66:291–294. [PubMed: 5038455]

Forbes JR, Hsi G, Cox DW. Role of the copper-binding domain in the copper transport function of ATP7B, the P-type ATPase defective in Wilson disease. J. Biol. Chem 1999;274:12408–12413. [PubMed: 10212214]

Frank J, Radermacher M, Penczek P, Zhu J, Li Y, Ladjadj M, Leith A. SPIDER and WEB: processing and visualization of images in 3D electron microscopy and related fields. J. Struct. Biol 1996;116:190–199. [PubMed: 8742743]

Gitschier J, Moffat B, Reilly D, Wood WI, Fairbrother WJ. Solution structure of the fourth metal-binding domain from the Menkes copper-transporting ATPase. Nat. Struct. Biol 1998;5:47–54. [PubMed: 9437429]

Harpaz Y, Gerstein M, Chothia C. Volume changes on protein folding. Structure 1994;2:641–649. [PubMed: 7922041]

Hatori Y, Majima E, Tsuda T, Toyoshima C. Domain organization and movements in heavy metal ion pumps: papain digestion of CopA, a Cu+-transporting ATPase. J. Biol. Chem 2007;282:25213–25221. [PubMed: 17616523]

Haupt M, Bramkamp M, Coles M, Altendorf K, Kessler H. Inter-domain motions of the N-domain of the KdpFABC complex, a P-type ATPase, are not driven by ATP-induced conformational changes. J. Mol. Biol 2004;342:1547–1558. [PubMed: 15364580]

Huster D, Lutsenko S. The distinct roles of the N-terminal copper-binding sites in regulation of catalytic activity of the Wilson's disease protein. J. Biol. Chem 2003;278:32212–32218. [PubMed: 12794172]

Jorgensen PL, Andersen JP. Structural basis for E_1-E_2 conformational transitions in Na,K-pump and Ca-pump proteins. J. Membr. Biol 1988;103:95–120. [PubMed: 3054114]

Kuhlbrandt W. Biology, structure and mechanism of P-type ATPases. Nat. Rev. Mol. Cell Biol 2004;5:282–295. [PubMed: 15071553]

Lee S, Kim YY, Lee Y, An G. Rice P1B-type heavy-metal ATPase, OsHMA9, is a metal efflux protein. Plant Physiol 2007;145:831–842. [PubMed: 17827266]

Lubben M, Guldenhaupt J, Zoltner M, Deigweiher K, Haebel P, Urbanke C, Scheidig AJ. Sulfate acts as phosphate analog on the monomeric catalytic fragment of the CPx-ATPase CopB from Sulfolobus solfataricus. J. Mol. Biol 2007;369:368–385. [PubMed: 17434529]

Lutsenko S, Barnes NL, Bartee MY, Dmitriev OY. Function and regulation of human copper-transporting ATPases. Physiol. Rev 2007;87:1011–1046. [PubMed: 17615395]

Lutsenko S, Kaplan JH. Organization of P-type ATPases: significance of structural diversity. Biochemistry 1995;34:15607–15613. [PubMed: 7495787]

Mana-Capelli S, Mandal AK, Arguello JM. *Archaeoglobus fulgidus* CopB is a thermophilic Cu^{2+}-ATPase: functional role of its histidine-rich-N-terminal metal binding domain. J. Biol. Chem 2003;278:40534–40541. [PubMed: 12876283]

Mandal AK, Arguello JM. Functional roles of metal binding domains of the Archaeoglobus fulgidus Cu^{+}-ATPase CopA. Biochemistry 2003;42:11040–11047. [PubMed: 12974640]

Mandal AK, Cheung WD, Arguello JM. Characterization of a thermophilic P-type Ag+/Cu+-ATPase from the extremophile *Archaeoglobus fulgidus*. J. Biol. Chem 2002;277:7201–7208. [PubMed: 11756450]

Mitra B, Sharma R. The cysteine-rich amino-terminal domain of ZntA, a Pb(II)/Zn(II)/Cd(II)-translocating ATPase from Escherichia coli, is not essential for its function. Biochemistry 2001;40:7694–7699. [PubMed: 11412123]

Moller JV, Juul B, le Maire M. Structural organization, ion transport, and energy transduction of P-type ATPases. Biophys. Bioch. Acta 1996;1286:1–51.

Moller JV, Olesen C, Jensen AM, Nissen P. The structural basis for coupling of Ca2+ transport to ATP hydrolysis by the sarcoplasmic reticulum Ca^{2+}-ATPase. J. Bioenerg. Biomembr 2005;37:359–364. [PubMed: 16691465]

Morgan CT, Tsivkovskii R, Kosinsky YA, Efremov RG, Lutsenko S. The distinct functional properties of the nucleotide-binding domain of ATP7B, the human copper-transporting ATPase: analysis of the Wilson disease mutations E1064A, H1069Q, R1151H, and C1104F. J. Biol. Chem 2004;279:36363–36371. [PubMed: 15205462]

Morth JP, Pedersen BP, Toustrup-Jensen MS, Sorensen TL, Petersen J, Andersen JP, Vilsen B, Nissen P. Crystal structure of the sodium-potassium pump. Nature 2007;450:1043–1049. [PubMed: 18075585]

Odermatt A, Suter H, Krapf R, Solioz M. Primary structure of two p-type ATPases involved in copper homeostasis in *Enterococcus hirae*. J. Biol. Chem 1993;268:12775–12779. [PubMed: 8048974]

Pedersen BP, Buch-Pedersen MJ, Morth JP, Palmgren MG, Nissen P. Crystal structure of the plasma membrane proton pump. Nature 2007;450:1111–1114. [PubMed: 18075595]

Petris MJ, Mercer JF, Culvenor JG, Lockhart P, Gleeson PA, Camakaris J. Ligand-regulated transport of the Menkes copper P-type ATPase efflux pump from the Golgi apparatus to the plasma membrane: a novel mechanism of regulated trafficking. EMBO J 1996;15:6084–6095. [PubMed: 8947031]

Pettersen EF, Goddard TD, Huang CC, Couch GS, Greenblatt DM, Meng EC, Ferrin TE. UCSF Chimera--a visualization system for exploratory research and analysis. J. Comput. Chem 2004;25:1605–1612. [PubMed: 15264254]

Pufahl RA, Singer CP, Peariso KL, Lin S-J, Schmidt PJ, Fahrni CJ, Culotta V. Cizewski, Penner-Han JE, O'Halloran TV. Metal ion chaperone function of the soluble Cu(I) receptor Atx1. Science 1997;278:853–856. [PubMed: 9346482]

Rensing C, Fan B, Sharma R, Mitra B, Rosen BP. CopA: An Escherichia coli Cu(I)-translocating P-type ATPase. Proc. Nat. Acad. Sci 2000;97:652–656. [PubMed: 10639134]

Rice WJ, Kovalishin A, Stokes DL. Role of metal-binding domains of the copper pump from *Archaeoglobus fulgidus*. Biochem. Biophys. Res. Commun 2006;348:124–131. [PubMed: 16876128]

Rice WJ, Young HS, Martin DW, Sachs JR, Stokes DL. Structure of Na^+,K^+-ATPase at 11 Å resolution: comparison with Ca^{2+}-ATPase in E_1 and E_2 states. Biophys. J 2001;80:2187–2197. [PubMed: 11325721]

Sazinsky MH, Agarwal S, Arguello JM, Rosenzweig AC. Structure of the actuator domain from the Archaeoglobus fulgidus Cu^+-ATPase. Biochemistry 2006a;45:9949–9955. [PubMed: 16906753]

Sazinsky MH, Mandal AK, Arguello JM, Rosenzweig AC. Structure of the ATP binding domain from the Archaeoglobus fulgidus Cu^+-ATPase. J. Biol. Chem 2006b;281:11161–11166. [PubMed: 16495228]

Schaefer M, Hopkins RG, Failla ML, Gitlin JD. Hepatocyte-specific localization and copper-dependent trafficking of the Wilson's disease protein in the liver. Am. J. Physiol 1999;276:G639–646. [PubMed: 10070040]

Sorensen TL, Møller JV, Nissen P. Phosphoryl transfer and calcium ion occlusion in the calcium pump. Science 2004;304:1672–1675. [PubMed: 15192230]

Stokes DL, Delavoie F, Rice WJ, Champeil P, McIntosh DB, Lacapere JJ. Structural studies of a stabilized phosphoenzyme intermediate of Ca^{2+}-ATPase. J. Biol. Chem 2005;280:18063–18072. [PubMed: 15734741]

Takahashi M, Kondou Y, Toyoshima C. Interdomain communication in calcium pump as revealed in the crystal structures with transmembrane inhibitors. Proc. Nat. Acad. Sci 2007;104:5800–5805. [PubMed: 17389383]

Toyoshima C, Inesi G. Structural basis of ion pumping by Ca^{2+}-ATPase of the sarcoplasmic reticulum. Annu. Rev. Biochem 2004;73:269–292. [PubMed: 15189143]

Toyoshima C, Mizutani T. Crystal structure of the calcium pump with a bound ATP analogue. Nature 2004;430:529–535. [PubMed: 15229613]

Toyoshima C, Nakasako M, Nomura H, Ogawa H. Crystal structure of the calcium pump of sarcoplasmic reticulum at 2.6 Å resolution. Nature 2000;405:647–655. [PubMed: 10864315]

Toyoshima C, Nomura H. Structural changes in the calcium pump accompanying the dissociation of calcium. Nature 2002;418:605–611. [PubMed: 12167852]

Toyoshima C, Nomura H, Tsuda T. Lumenal gating mechanism revealed in calcium pump crystal structures with phosphate analogues. Nature 2004;432:361–368. [PubMed: 15448704]

Toyoshima C, Unwin N. Three-dimensional structure of the acetylcholine receptor by cryoelectron microscopy and helical image reconstruction. J. Cell. Biol 1990;111:2623–2635. [PubMed: 2277076]

Toyoshima C, Yonekura K, Sasabe H. Contrast transfer for frozen-hydrated specimens: II. Amplitude contrast at very low frequencies. Ultramicroscopy 1993;48:165–176.

Tsivkovskii R, MacArthur BC, Lutsenko S. The Lys1010-Lys1325 fragment of the Wilson's disease protein binds nucleotides and interacts with the N-terminal domain of this protein in a copper-dependent manner. J. Biol. Chem 2001;276:2234–2242. [PubMed: 11053407]

Vulpe CD, Packman S. Cellular copper transport. Annu. Rev. Nutr 1995;15:293–322. [PubMed: 8527222]

Wernimont AK, Huffman DL, Lamb AL, O'Halloran TV, Rosenzweig AC. Structural basis for copper transfer by the metallochaperone for the Menkes/Wilson disease proteins. Nat. Struct. Biol 2000;7:766–771. [PubMed: 10966647]

Williams LE, Mills RF. P(1B)-ATPases--an ancient family of transition metal pumps with diverse functions in plants. Trends Plant Sci 2005;10:491–502. [PubMed: 16154798]

Xu C, Rice WJ, He W, Stokes DL. A structural model for the catalytic cycle of Ca^{2+}-ATPase. J. Mol. Biol 2002;316:201–211. [PubMed: 11829513]

Yoshimizu T, Omote H, Wakabayashi T, Sambongi Y, Futai M. Essential Cys-Pro-Cys motif of Caenorhabditis elegans copper transport ATPase. Biosci. Biotechnol. Biochem 1998;62:1258–1260. [PubMed: 9692213]

Yuan DS, Dancis A, Klausner RD. Restriction of copper export in Saccharomyces cerevisiae to a late Golgi or post-Golgi compartment in the secretory pathway. J. Biol. Chem 1997;272:25787–25793. [PubMed: 9325307]

Zhang P, Toyoshima C, Yonekura K, Green NM, Stokes DL. Structure of the calcium pump from sarcoplasmic reticulum at 8 Å resolution. Nature 1998;392:835–839. [PubMed: 9572145]

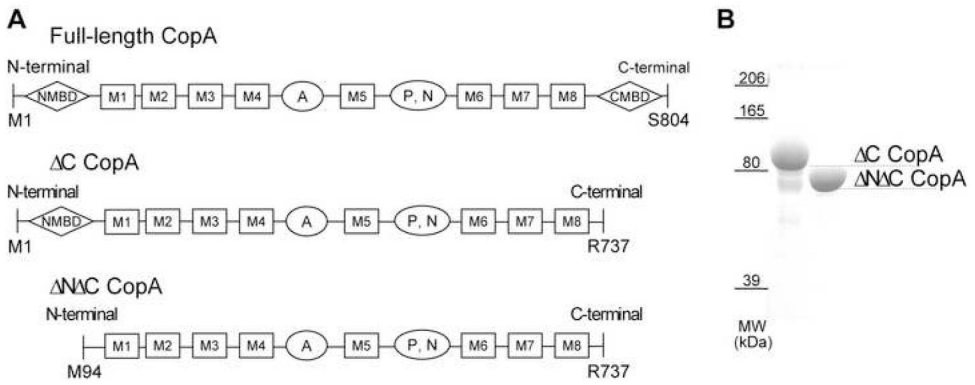

Figure 1.

Constructs of CopA used for crystallization. (A) Domain organization of constructions with MBDs indicated by diamonds, transmembrane helices by rectangles and cytoplasmic domains by ovals. Residues at the beginning and end of each construct are indicated, with ΔC-CopA and ΔNΔC-CopA being used here for crystallization. (B) Coomassie stained SDS polyacrylamide gel of the purified protein used for crystallization.

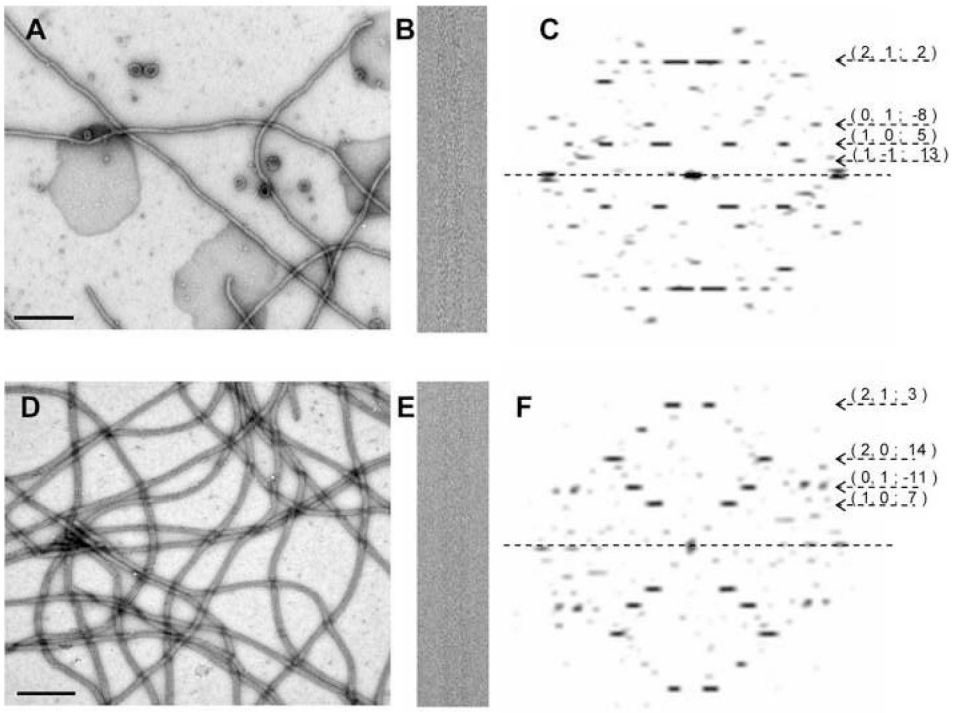

Figure 2.

Tubular crystals of CopA. (A,B,C) Raw data for ΔC-CopA with a low magnification image of negatively stained samples (A), a higher magnification image of an individual frozen-hydrated tube and (C) its Fourier transform. (D,E,F) Analogous data for ΔNΔC-CopA. Scale bar in negatively stained images corresponds to 0.5 μm. Numbers beside the Fourier transforms indicate the Miller indices of selected layer lines together with their assigned Bessel order, which are visible to ~25 Å.

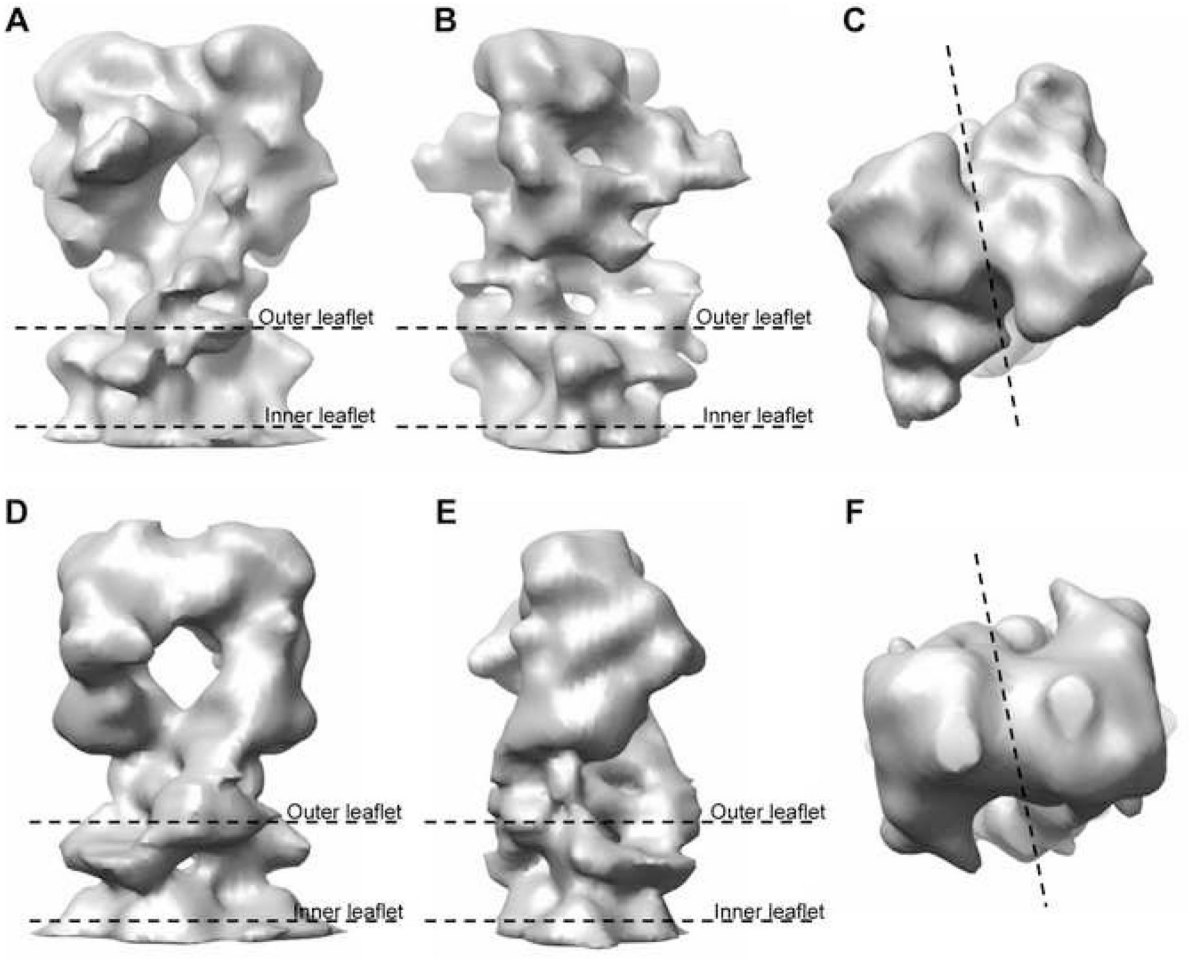

Figure 3.

3D reconstruction of CopA. (A,B,C) Three orthogonal views of the ΔC-CopA dimer that composes the unit cell. (D,E,F) Analogous views of the ΔNΔC-CopA dimer. The boundary of the membrane is indicated in side views with "outer leaflet" referring to the outer surface of the tube (Supplementary Figure 1). The dotted line in c and f shows the boundary between the monomers.

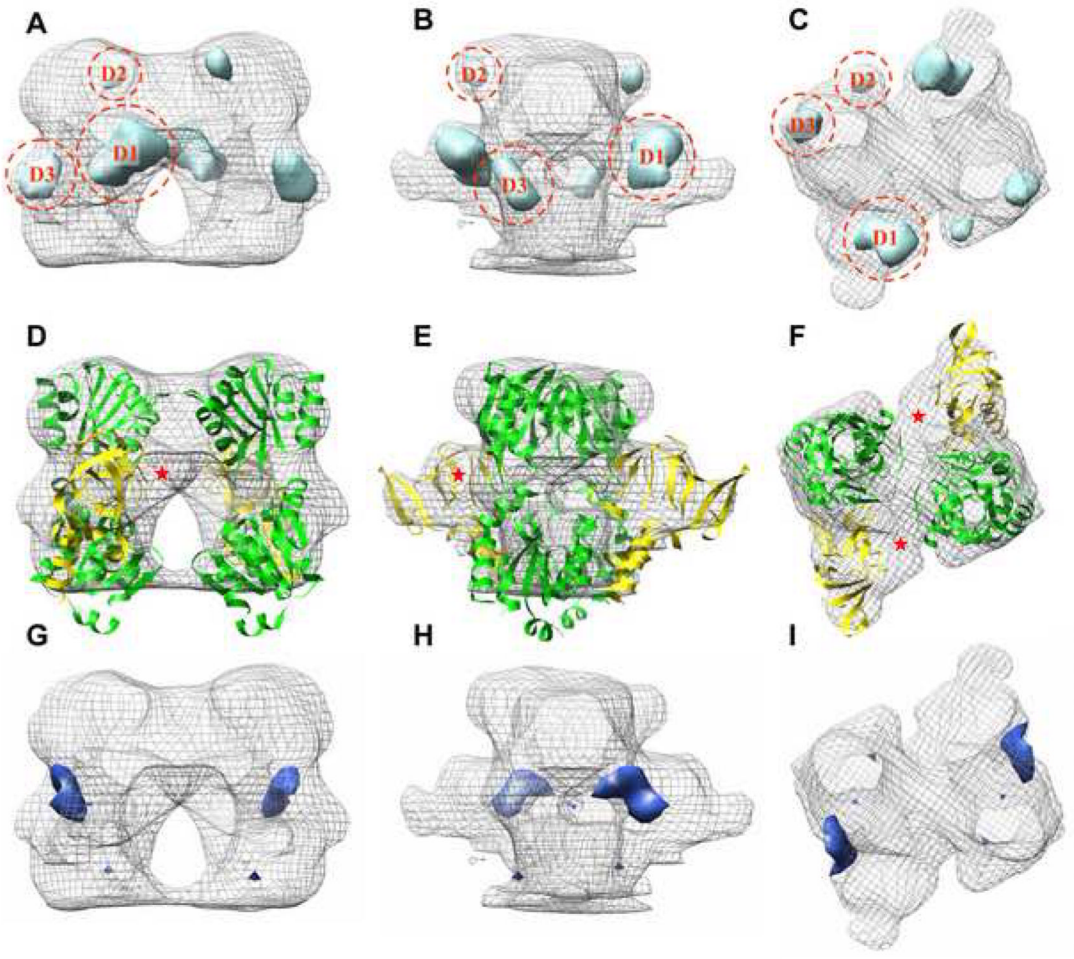

Figure 4.

Difference map for ΔC-CopA minus ΔNΔC-CopA. (A,B,C) Positive difference densities (light blue) plotted at 2.5σ superimposed on the envelope of ΔC-CopA (grey mesh). (D,E,F) Fitting of cytoplasmic domains to the envelope of ΔC-CopA, revealing an unoccupied region that likely corresponds to the N-terminal MBD (red asterick). (G,H,I) A single negative difference density at 2.5σ from the difference map (dark blue). Views are as in Figure 3.

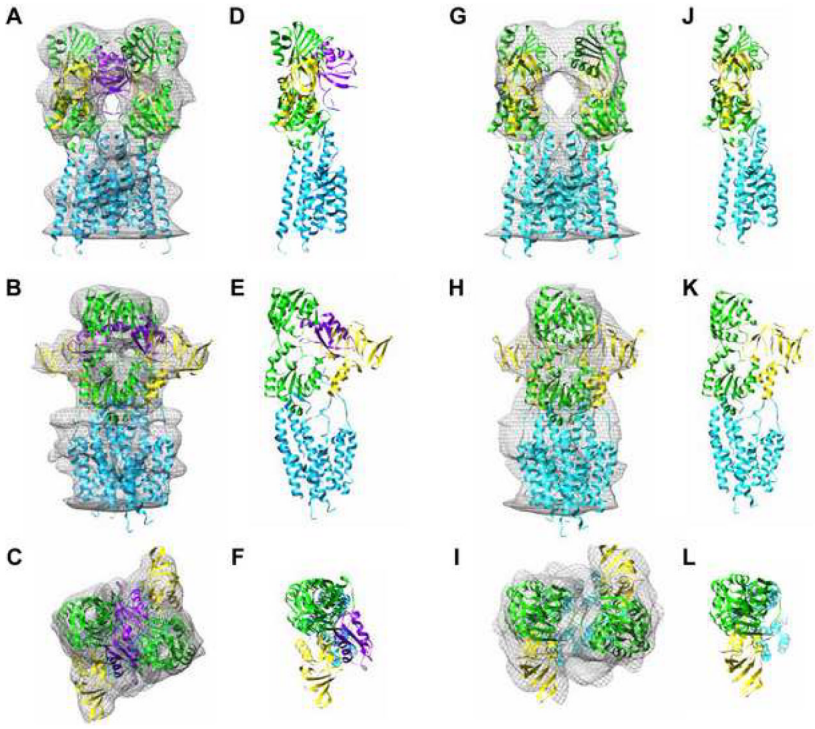

Figure 5.
Atomic model for CopA docked to the maps. (A-F) Model for ΔC-CopA. (G-L) Model for ΔNΔC-CopA. Domains have been colored as follows: transmembrane helices (cyan), P-/N-domain (green), A-domain (yellow), N-terminal MBD (magenta).

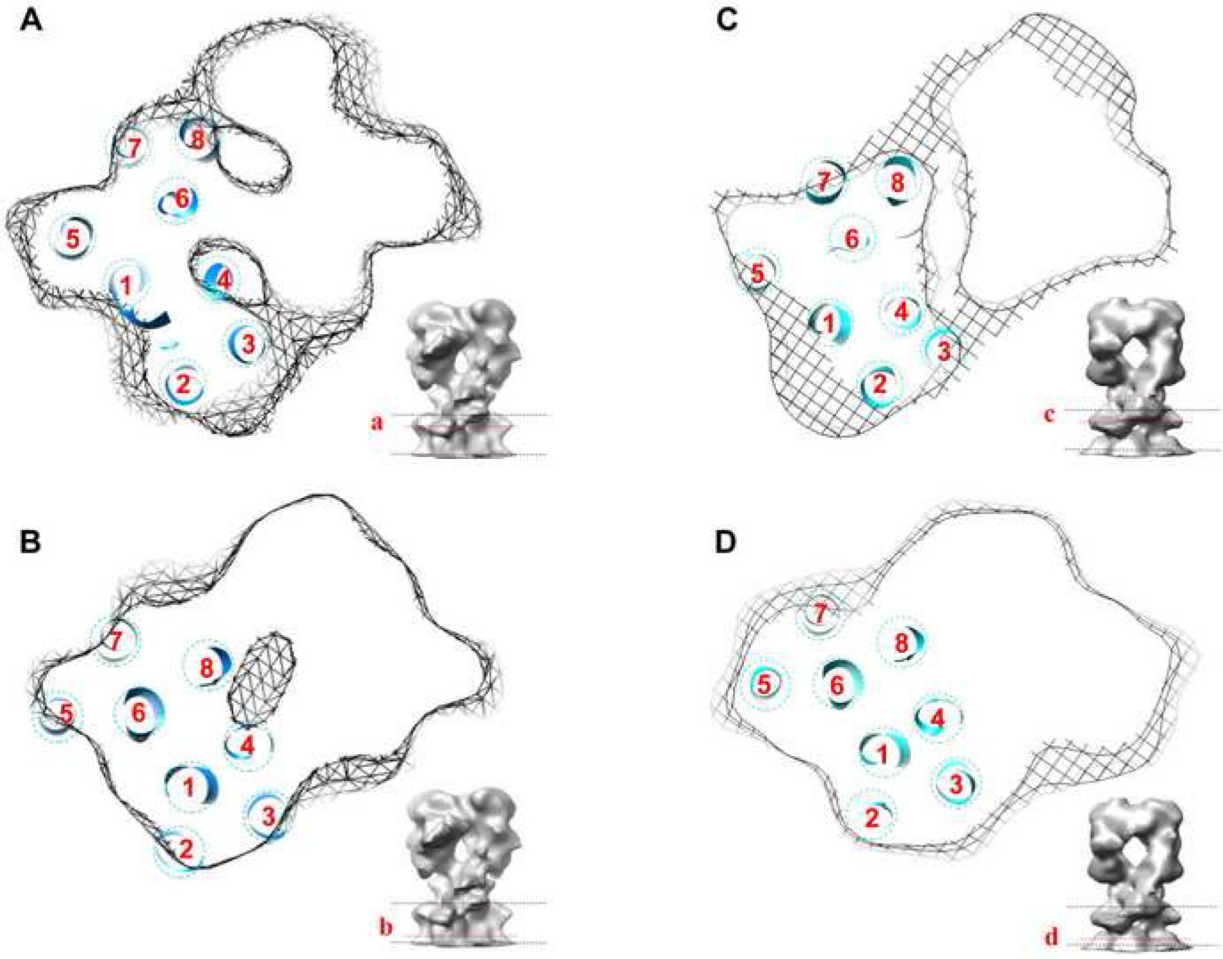

Figure 6.

Location of the transmembrane helices of CopA. (A,B) Helices are shown fitted to one monomer of the ΔC-CopA dimer in two sections near the top (A) and bottom (B) of the membrane. (C,D) ΔNΔC-CopA helices at similar locations in the membrane, which are indicated in the inset to each panel. The arrangement of helices and their location relative to the P-domain was the same in both models and slight differences in appearance reflect a slightly different depth of the respective sections within the membrane.

Figure 7.

Interactions between the cytoplasmic domains. The N-terminal MBD (magenta) is shown interacting with both the A-domain (yellow) and the ATP-binding N-domain (green). Several residues from the MBD implicated in recognizing the metallochaperone are shown in ball and stick representation in magenta and the conserved, metal-liganding cysteine residues from the MBD are shown in ball and stick representation in yellow (sequence numbers corresponds to *B. subtilis*). The conserved Glu and His from an ATP-binding loop of the CopA N-domain are also shown in ball and stick representation in green, near the site of interaction with the MBD (sequence numbers corresponds to *A. fulgidus*). This view is roughly the same as Figure 5f.

Table I

Statistics of data averaging

		ΔC CopA	ΔNΔC CopA
n (1,0)		5	7
n (0,1)		-8	-11
no. of tubes		11	13
no of dimers		2397	5873
unit cell dimensions	a (Å)	75 ± 1.1	71.2 ± 1.5
	b (Å)	47 ± 0.7	47.4 ± 0.7
	γ (°)	69.9 ± 0.8	65.9 ± 0.9
two-fold phase residual[a]	∞-35Å (°)	7.9	6.5
	35-25Å (°)	10.4	10.0
	25-20Å (°)	29.5	31.3
	20-17.5Å (°)	39.0	38.9
	17.5-15Å (°)	40.2	41.6
FSC[b]	0.5 (Å)	17.3	17.5
	0.3 (Å)	14.8	15.9

[a] Phase residual in the indicated resolution bins.

[b] Resolution at which the Fourier Shell Coefficient falls to the indicated value.